Modeling the Dynamics of Centerless Mortise Grinding on Rigid Supports

Vasyl Chalyj[1], Serhii Moroz[2], Anatolii Tkachuk[2(✉)], Valentyn Zablotskyi[2], and Oleg Zabolotnyi[2]

[1] PSC «SKF Ukraine», 34, Bozhenka St., Lutsk 43017, Ukraine
[2] Lutsk National Technical University, 75, Lvivska St., Lutsk 43018, Ukraine
a.tkachuk@lntu.edu.ua

Abstract. The paper examines the influence of the dynamic parameters of the machine and the geometry of the adjustment of rigid supports on the formation of undulations of the surfaces of roller bearing rings. A complex mathematical model of the machine tool system for centerless mortise grinding was developed, and the influence of the dynamic parameters of the machine tool and the geometry of the setup of rigid supports on the formation of undulations of the processed surfaces was analyzed. The SWaAGL-50 mortise centerless grinding machine's technological system is presented as a linear mechanical model, and the elastic movements along the OX axis are considered. Based on the equations of kinetic and potential energies compiled in the form of Lagrange, the equations of motion of the relevant elements of the technological system were obtained. The formula of the dynamic accuracy function was found, which characterizes the inconsistency of the movement of the grinding wheel and the part.

Keywords: Mathematical Modeling · SWaAGL-50 Machine · Resonant Frequencies · Hodograph · Stability Trends

1 Introduction

The modern level of development of bearing production necessitates the creation and implementation of technological processes, the application of which provides the necessary indicators of the operational properties of roller bearing parts [1]. The operational properties of roller bearings determine the competitiveness of mechanical engineering products [2]. They depend on the state of their working surfaces, which are characterized by a set of geometric and physical-mechanical quality parameters that are formed during the finishing operations of technological processes of mechanical processing [3].

Among the finishing operations, types of grinding are used, which make it possible to ensure high dimensional accuracy and the quality of the processed surface [4]. The study of the mechanism of the formation of parameters of the state of the working surface being processed is an urgent issue in the theory and practice of grinding [5]. For the analysis and research of grinding processes, mathematical models are used in which Laplace operators are used for the analysis of the centerless grinding system. In such

V. Tonkonogyi et al. (Eds.): Interpartner 2024, LNME, pp. 253–265, 2025.
https://doi.org/10.1007/978-3-031-82746-4_23

models, it is necessary to consider the technological system for grinding as a whole, considering the machine's characteristics, the tools, and the part being processed [6].

The purpose of the research: to develop a complex mathematical model of the SWaAGL-50 centerless mortise grinding machine, to analyze the influence of the dynamic parameters of the machine and the geometry of the adjustment of rigid supports on the formation of the waviness of the detail surfaces.

2 Literature Review

Research on the process of centerless grinding was carried out in the paper [7, 8], various approaches were used, and various parameters and indicators of the process were considered. In particular, the analysis carried out in [9] assumed that the part, rigid supports, grinding wheel, and machine were perfectly rigid. However, the machine-tool-part (MTP) process system is flexible and causes vibrations over the entire frequency range during normal operation in the manufacturing process. In paper [8, 10] static or stability forces were considered. However, for a complete understanding of the behavior of the technological system, efforts must be made to model the machine and find its influence on the technological process [11].

The strategy here is to create an adequate machine tool model in the Laplace domain to analyze the machine tool displacement hodograph with the combined displacement hodograph from papers [7, 12] in the complex plane, and then compare different $s = \sigma + j_n$ between tuning conditions. Machine vibration affects the final accuracy of the manufactured part in three ways [13, 14]. The static stiffness of the machine affects the dimensional accuracy of the part of the grinding forces, excites oscillations in the machine, and leads to false dimensional feedback. The geometric influence considered will be strengthened or weakened depending on the low resonant frequencies of the machine. It should be taken into account that higher frequency resonances of the machine generate high-frequency irregularities on the surface of the part, apart from the geometric regeneration mechanism. These mechanisms can be described by observing the frequency spectrum of oscillations with the corresponding growth rates in the s zone. In the Laplace area, the effects created by the machine will be combined with the effects found in the papers [8].

By analyzing the hodograph of the movement of the machine with the combined hodograph of the movement of waviness and regeneration at a given frequency, the solution of the systems of characteristic equations graphically determines the rate of growth of dynamic vibrations. This graphical coincidence will allow us to compare different tuning geometries in terms of the unstable exponential growth of σ in $s = \sigma + j_n$.

3 Research Methodology

3.1 Mathematical Model of a Machine for Centerless Mortise Grinding on Rigid Supports

Grinding machines are made up of individual components, including motors, feed mechanisms, bearings, grinding wheels, etc. Each of these components resonates at one or more separate frequencies [7]. Machine components are solid structures that can be

modeled as discrete sets of individual elements consisting of linear springs, masses, and dampers. Each set of modeling elements has its characteristic equation, and they were all combined in the Laplace domain to obtain Eq. (1):

$$H(s) = \sum_{n=1}^{m} \frac{\omega_n^2}{s^2 + 2\xi\omega_n s + \omega_n^2}. \tag{1}$$

The value of m in Eq. (1) in reality reaches infinity, but most of the main effects of the machine are found when m is small and limited. This approach assumes that the machine is made of linear springs and that any non-linear element is linearized for the model.

As noted in paper [8], forced oscillations of technological system elements play the greatest role in the formation of waviness. We will present the MTP system of a mortise centerless grinding machine, for example, the SWaAGL-50 model, in the form of a linear mechanical model (Fig. 1) and consider elastic movements along the *OX* axis.

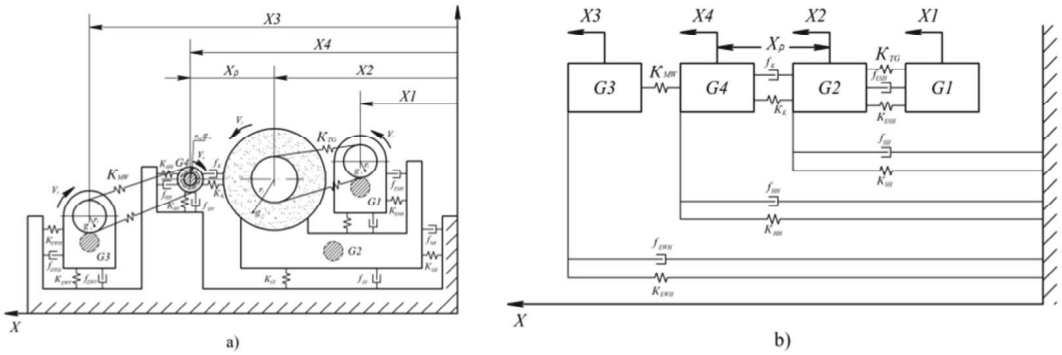

Fig. 1. Mechanical model (a) and dynamic diagram (b) of the machine-part system during centerless grinding on the SWaAGL-50 machine.

The equations of motion for each coordinate in the Lagrange form have the form:

$$\frac{d}{dt}\frac{\partial L}{\partial \dot{x}} - \frac{\partial L}{\partial x} = Q, \tag{2}$$

where $i = 1, 2 \ldots n$; Q_i – generalized non-potential force; $L = W_{kin} - W_{pot}$; W_{kin}– kinetic energy of the system; W_{pot} – potential energy of the system.

After appropriate substitutions and transformations, we get a system of n equations:

$$\sum_{k=1}^{n} g_{ik}\ddot{x}_k + f_{ik}\dot{x}_k + c_{ik}x_k = A_k \cos(\phi_k + \upsilon_k t) \tag{3}$$

where g, f, c are mass coefficients, damping coefficients, stiffness coefficients according too,

$$A_k = z_k \cdot \upsilon_k^2 \tag{4}$$

where z – imbalance of rotating system elements; ν – frequency of rotation of imbalances; ϕ – oscillation phases.

The relative forced oscillations of the part and the grinding wheel are characterized by the dynamic accuracy function, which is the sum of partial solutions for each coordinate

$$x_p(t) = \sum_{k=1}^{n} \frac{1}{\upsilon_k} \alpha_p^{\upsilon_k} \sin\left(\upsilon_k t + \phi_p^{\upsilon_k}\right) + \sum_{l=1}^{n} \frac{1}{\omega_l} \beta_p^{\omega_l} sin\left(\omega_l t + \phi_p^{\omega_l}\right) \tag{5}$$

where ν, ω are the frequencies of forced and free oscillations of the elements, respectively; α_p, β_p are functions that depend on the structure of the system and the connections of elements.

In the linear model of the MTP system of the SWaAGL-50 machine, the following conventions and assumptions are adopted: 1) the movement of the inertial element in the inertial frame of reference takes place in one direction, along the OX axis; 2) the support is a body (machine or earth), which has such a large mass that the reverse action of the elements oscillating on the support can be neglected; 3) the support, inertial element and elements that serve to secure the springs are not deformed; 4) we neglect the mass of elastic suspensions; 5) the elastic force is proportional to the deformation of the elastic suspension; 6) the viscous resistance in the system is proportional to the first step of the displacement speed of the inertial element; 7) mass, stiffness coefficient, damping coefficient are constant parameters that do not change in the studied period; 8) the beginning of the displacement count is chosen at the position of the center of mass at equilibrium.

In Fig. 1, the following designations are used: G_1 – mass of the electric motor driving the circle with the plate; G_2 – mass of the table with the grinding headstock; G_3 – weight of the electric motor of the drive of the product with the plate; G_4 – weight of the part; g_1, g_2, g_3, g_4 – unbalanced masses of the rotor of the electric motor driving the wheel, the spindle with the grinding wheel, the rotor of the electric motor driving the product and the part, respectively; r_1, r_2, r_3, r_4 – radius of location of unbalanced masses; K_{ESH}, K_{SH}, K_{EWH}, K_{HH}, K_{ESV}, K_{SV}, K_{EWV}, K_{HV} – horizontal and vertical stiffness coefficients of the corresponding elements according to the scheme; K_{TG} – stiffness coefficient of the belt transmission of the grinding wheel; K_{MW} – stiffness coefficient of the magnetic transmission of the workpiece drive; K_K – stiffness coefficient of contact between the surfaces of the grinding wheel and the processed workpiece; f_H, f_V – horizontal and vertical damping coefficients, respectively; x_1, x_2, x_3, x_4 – displacement of the corresponding elements according to the scheme; x_p is the coordinate of the misalignment of the contact between the working surface of the circle and the polished surface of the part.

Based on the equations of kinetic and potential energies compiled in the form of Lagrange, by entering the appropriate notations:

$$K_{ESH} + K_{TG} = k_1, \qquad g_1 + G_1 = g'_1,$$

$$K_{SH} + K_K = k_2, \qquad g_2 + G_2 = g'_2,$$

$$K_{EWH} + K_{MW} = k_3, \qquad g_3 + G_3 = g'_3,$$

$$K_{HH} + K_K = k_4, \qquad g_4 + G_4 = g'_4,$$

we obtain the equations of motion of the corresponding elements.

$$\acute{g}_1(\ddot{x}_1 + \ddot{x}_2) + k_1 x_1 = -g_1 r_1 v_1^2 cos(\phi_1^0 + \nu_1 t) \tag{6}$$

$$\acute{g}_1(\ddot{x}_1 + \ddot{x}_2) + \acute{g}_2\ddot{x}_2 - K_{HH}\ddot{x}_2 + k_2 x_2 - K_C x_4 = -g_1 r_1 v_1^2 cos(\phi_1^0 + \nu_1 t) - g_2 r_2 v_2^2 cos(\phi_2^0 + \nu_2 t) \tag{7}$$

$$\acute{g}_3(\ddot{x}_3 + \ddot{x}_4) + k_3 x_3 = -g_3 r_3 v_3^2 cos(\phi_1^0 + \nu_1 t) \tag{8}$$

$$\acute{g}_3(\ddot{x}_3 + \ddot{x}_4) + \acute{g}_4\ddot{x}_4 - K_{HH}\ddot{x}_4 - k_4 x_4 - K_C x_4 = -g_3 r_3 v_3^2 cos(\phi_3^0 + \nu_3 t) - g_4 r_4 v_4^2 cos(\phi_4^0 + \nu_4 t) \tag{9}$$

Subtracting Eq. (6) from (7) and Eq. (8) from (9), we get:

$$\acute{g}_2\ddot{x}_2 + K_{SH}\ddot{x}_2 + k_2 x_2 - k_1 x_1 - K_C x_4 = -g_2 r_2 v_2^2 cos(\phi_2^0 + \nu_2 t)$$

$$\acute{g}_4\ddot{x}_4 + K_{SH}\ddot{x}_4 + k_4 x_4 - k_3 x_3 - K_C x_2 = -g_4 r_4 v_4^2 cos(\phi_4^0 + \nu_4 t)$$

Having found $\ddot{x}_2$ and $\ddot{x}_4$, substituting their values into Eqs. (6) and (8), respectively, let's convert Eqs. (6)–(9) into the form:

$$\left.\begin{aligned}
\ddot{x}_1 + \left(\tfrac{k_1}{\acute{g}_1} + \tfrac{k_1}{\acute{g}_2}\right)x_1 - \tfrac{K_{SH}}{\acute{g}_2}\acute{x}_2 - \tfrac{k_1}{\acute{g}_2}x_2 + \tfrac{K_C}{\acute{g}_2}x_1 &= -\tfrac{g_1}{\acute{g}_1}r_1 v_1^2 cos(\phi_1^0 + \nu_1 t) + \tfrac{g_2}{\acute{g}_2}r_2 v_2^2 cos(\phi_2^0 + \nu_2 t)\\
\ddot{x}_2 + \tfrac{K_{HH}}{\acute{g}_2}\acute{x}_2 + \tfrac{k_2}{\acute{g}_2} - \tfrac{k_1}{\acute{g}_2}x_1 + \tfrac{k_2}{\acute{g}_2}x_4 &= -\tfrac{g_2}{\acute{g}_2}r_2 v_2^2 cos(\phi_2^0 + \nu_2 t)\\
\ddot{x}_3 + \left(\tfrac{k_3}{\acute{g}_3} + \tfrac{k_3}{\acute{g}_4}\right)x_3 - \tfrac{K_{HH}}{\acute{g}_4}\acute{x}_4 - \tfrac{k_4}{\acute{g}_4}x_4 &= -\tfrac{g_3}{\acute{g}_4}r_3 v_3^2 cos(\phi_3^0 + \nu_3 t) + \tfrac{g_4}{\acute{g}_4}r_4 v_4^2 cos(\phi_4^0 + \nu_4 t)\\
\ddot{x}_4 + \tfrac{K_{HH}}{\acute{g}_4}\acute{x}_4 + \tfrac{k_3}{\acute{g}_4}x_3 + \tfrac{k_3}{\acute{g}_4}x_2 &= \tfrac{g_4}{\acute{g}_4}r_4 v_4^2 cos(\phi_4^0 + \nu_4 t)
\end{aligned}\right\} \tag{10}$$

In expression (10), a system of linear inhomogeneous differential equations of the 2nd order is obtained, which describe the movement of the elements of the MTP system of the SWaAGL-50 machine. Each of the right-hand parts of this system $g_i r_i v_i^2 cos(\phi_i^0 + \nu_i t)$ represents a centrifugal force caused by the imbalance of the corresponding mass at $i = 1$, 2, 3, 4. During fine grinding, and especially during finishing, the influence of secondary sources will be very small, so it can be neglected by taking $x_i = \alpha_i e^{pi}$; $\dot{x}_i = \alpha_i p e^{pi}$; $\ddot{x}_i = \alpha_i p^2 e^{pi}$, where p – some number.

After substituting the accepted assumption into the equation of system (10) and transformations, we get:

$$\left.\begin{aligned}
\left[p^2 + \left(\tfrac{k_1}{\acute{g}_1} + \tfrac{k_1}{\acute{g}_2}\right)\right]\alpha_1 - \left(\tfrac{K_{HH}}{\acute{g}_2}p + \tfrac{k_2}{\acute{g}_2}\right)\alpha_2 + \tfrac{K_C}{\acute{g}_2}\alpha_4 &= 0;\\
-\tfrac{k_1}{\acute{g}_2}\alpha_1 + \left[p^2 + \left(\tfrac{K_{SH}}{\acute{g}_2}p + \tfrac{k_2}{\acute{g}_2}\right)\right]\alpha_2 + \tfrac{K_C}{\acute{g}_2}\alpha_4 &= 0;\\
\tfrac{K_C}{\acute{g}_2}\alpha_2 + \left[p^2 + \left(\tfrac{k_3}{\acute{g}_3} + \tfrac{k_3}{\acute{g}_4}\right)\right]\alpha_3 - \left(\tfrac{K_{HH}}{\acute{g}_2}p + \tfrac{k_2}{\acute{g}_2}\right)\alpha_2 &= 0;\\
-\tfrac{K_C}{\acute{g}_2}\alpha_2 - \tfrac{k_3}{\acute{g}_4}\alpha_3 + \left[p^2 + \left(\tfrac{K_{HH}}{\acute{g}_4}p + \tfrac{k_4}{\acute{g}_4}\right)\right]\alpha_4 &= 0.
\end{aligned}\right\} \tag{11}$$

$$\Delta(p) = p^8 + Ap^7 + Bp^6 + Cp^5 + Dp^4 + Ep^3 + Fp^2 + Lp + N$$

In this way, a characteristic equation of the 8th degree is obtained, all the coefficients of which are positive, since:

$$k_2k_4 + K_C^2 > 0;$$
$$k_2k_4 = (K_{SH} + K_C)(K_{HH} + K_C) = K_{SH}K_{HH} + K_C(K_{SH} + K_{HH}) + K_C^2;$$
$$k_2k_4 - K_C^2 = K_{SH}K_{HH} + K_C(K_{SH} + K_{HH}) > 0.$$

As a result, the characteristic equation has no real roots. All eight roots are complex, that is, they have four pairs of complex conjugate roots. They have the following form:

$$\begin{cases} p_1 = -\delta_1 + i\omega_1; \\ p_2 = -\delta_1 - i\omega_1; \end{cases} \begin{cases} p_3 = -\delta_2 + i\omega_2; \\ p_4 = -\delta_2 - i\omega_2; \end{cases} \begin{cases} p_5 = -\delta_3 + i\omega_3; \\ p_6 = -\delta_3 - i\omega_3; \end{cases} \begin{cases} p_7 = -\delta_4 + i\omega_4; \\ p_8 = -\delta_4 - i\omega_4. \end{cases}$$

To find the roots, the characteristic equation should be solved. The task is to find system solutions (10) that satisfy the initial conditions:

$$\begin{gathered} \frac{x_2}{t=t_0} = x_2^0; \frac{x_3}{t=t_0} = x_3^0; \frac{x_4}{t=t_0} = x_4^0. \\ \frac{\dot{x}_1}{t=t_0} = \dot{x}_1^0; \frac{\dot{x}_2}{t=t_0} = \dot{x}_2^0; \frac{\dot{x}_3}{t=t_0} = \dot{x}_3^0; \frac{\dot{x}_4}{t=t_0} = \dot{x}_4^0. \end{gathered} \tag{12}$$

After transforming the system (10) with the initial conditions (12) using direct and inverse Laplace transformations, after carrying out a series of manipulations, the vibration displacement of the center of the part along the x_1 coordinate was obtained in the form:

$$x_1(t) = \frac{1}{\omega_1}\alpha_1^{\omega_1} e^{-\delta_1 t}\sin\left(\omega_1 t + \phi_1^{\omega_1}\right) + \frac{1}{v_1}\alpha_1^{v_1} e^{-\delta_1 t}\sin\left(v_1 t + \phi_1^{v_1}\right) \tag{13}$$

where $\alpha_1 = \sqrt{\frac{\alpha^2+b^2}{c^2+d^2}}$; $\phi_1 = arctg\,\frac{cb-ad}{ac+bd}$.

Expressions for the vibration displacements of the remaining elements 2, 3, and 4 of the MTP system are similarly found. Then, the formula of the function of dynamic accuracy, which characterizes the inconsistency of the movement of the grinding wheel and the part, that is, as the difference $x_p(p) = x_4(t) - x_2(t)$, will have the form:

$$\begin{gathered} x_p(t) = \frac{1}{\omega_1}\alpha_p^{\omega_1} e^{-\delta_1 t} sin\left(\omega_1 t + \phi_p^{\omega_1}\right) + \frac{1}{\omega_2}\alpha_p^{\omega_2} e^{-\delta_2 t} sin\left(\omega_2 t + \phi_p^{\omega_2}\right) \\ + \frac{1}{\omega_3}\alpha_p^{\omega_3} e^{-\delta_3 t} sin\left(\omega_3 t + \phi_p^{\omega_3}\right) + \frac{1}{\omega_4}\alpha_p^{\omega_4} e^{-\delta_4 t} sin\left(\omega_4 t + \phi_p^{\omega_4}\right) + \frac{1}{v_1}\alpha_p^{v_1} e^{-\delta_1 t} sin\left(v_1 t + \phi_p^{v_1}\right) \\ + \frac{1}{v_2}\alpha_p^{v_2} e^{-\delta_2 t} sin\left(v_2 t + \phi_p^{v_2}\right) + \frac{1}{v_3}\alpha_p^{v_3} e^{-\delta_3 t} sin\left(v_3 t + \phi_p^{v_3}\right) + \frac{1}{v_4}\alpha_p^{v_4} e^{-\delta_4 t} sin\left(v_4 t + \phi_p^{v_4}\right). \end{gathered} \tag{14}$$

The first four terms characterize the free oscillations of the system elements, which decay over time and therefore, if necessary, they can be neglected. The SWaAGL-50 machine for centerless slot grinding on rigid supports is a typical machine for the bearing industry. An accelerometer and an «Agilent HP 35665A Dynamic Signal Analyzer» signal analyzer were used to determine the resonant frequencies of the machine. Dynamic and static readings were taken from the machine, and the accelerometer was located in different areas of the machine to monitor the vibration of each of the above elements.

Table 1. Oscillation frequencies of SWaAGL-50 machine components.

Component	The value of the natural frequency, Hz	Component	The value of the natural frequency, Hz
Grinding wheel feeding support	48.8	Detail	525
Contact stiffness	82.5	Rigid supports (both)	735
Grinding wheel spindle	194	Grinding wheel	1950

For the off-machine tests, a piezoelectric hammer was used to simulate the forced pulses. Although any particular resonance is difficult to isolate, the strategic placement of the accelerometer relatively isolated a particular component of resonant frequencies.

Figure 2a shows the vibration spectrum of grinding wheel feeding support, Fig. 2b shows a logarithmic amplitude-frequency characteristic of grinding wheel feeding support, and Fig. 2c demonstrates the phase-frequency characteristic of grinding wheel feeding support. Analyzing the vibrations, the resonance frequencies of the components were estimated as shown in Table 1.

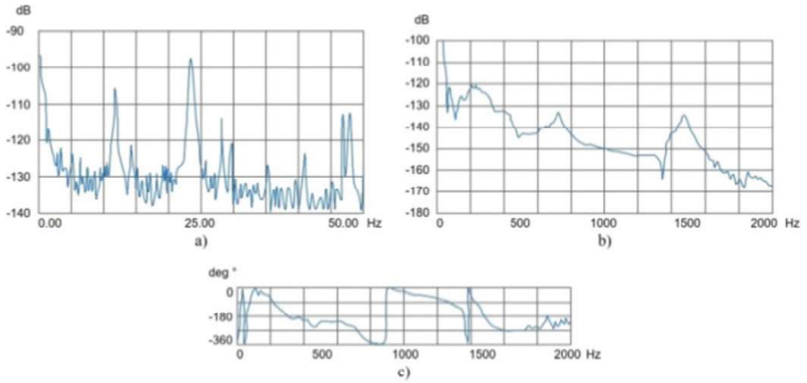

Fig. 2. Results of experiments of machine vibration.

According to the results of research on this machine, an experimental logarithmic amplitude-frequency characteristic was constructed (Fig. 3), and frequency response was based on the mathematical model of the machine (Fig. 4).

The simulation was performed in the Matlab environment, as a result of the characteristic equation, the logarithmic amplitude-frequency characteristics are shown in Fig. 5, which are very similar to the graphs in Fig. 4. Since the linear model has internal connections, we changed the components individually to find their effect on the amplitude-frequency characteristic. As can be seen from Fig. 4, only some of the resonant frequencies dominate the dynamic characteristics of the machine. The resonance of the machine bed and grinding wheel feed caliper were the main vibration components of this machine [7]. The results may vary depending on the model of the machine, but the general conclusion of dynamic stability for centerless mortise grinding on rigid supports

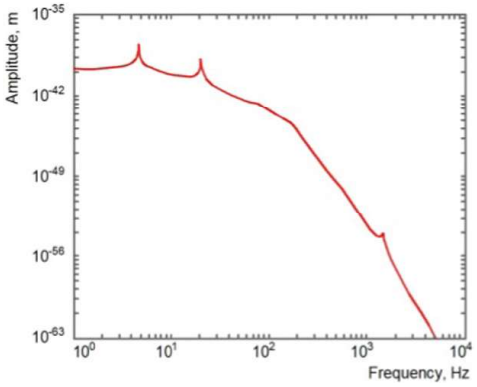

Fig. 3. Frequency response equation of the machine based on vibration parameters.

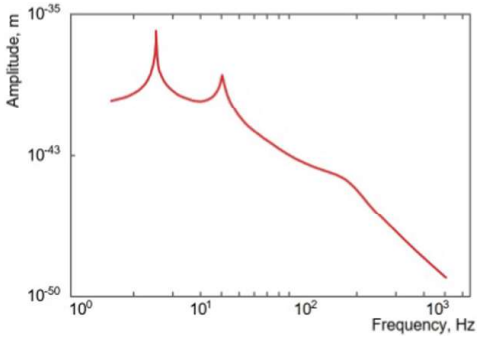

Fig. 4. Frequency response based on the mathematical model of the machine.

remains the same. The conclusion from the modeling shows that this machine can be effectively modeled from the characteristic Eq. (14).

3.2 Analysis of the Dependence of the Dynamic Stability of the Machine on the Geometry of the Adjustment of Rigid Supports

Since the exact mathematical solution is difficult, the value was found by the graphical matching method. After constructing the hodograph of the movement of the machine in the complex plane, as well as the hodograph of the movement of the mechanism of rigid supports (the combined hodograph of the movement of waviness and regeneration), the frequency and growth rate at which they coincide graphically were established. That is, the graphic coincidence has reached the frequency and σ values which are suitable for both hodographs, and the dynamic root of the system has also been established.

Dynamic analysis is best done by finding the roots of the system because the roots of the system fully characterize its stability. Based on the comparison of system roots under different debugging conditions, a dynamic stability diagram based on debugging conditions is developed. As it was established in [8], for any specific adjustment condition, the helix of the waviness displacement and regeneration hodograph for a specific harmonic can be adjusted in size by changing the exponential growth rate σ. The purpose of this analysis was to select a certain frequency on the hodograph of the movement of the machine and find the harmonic (the number of protrusions multiplied by the revolutions of the part per second) that corresponds to it. Then, the value of σ was adjusted to the intersection of both hodographs on the complex plane. The final value of σ could be positive or negative depending on the particular harmonic, and the exact frequency was adjusted to find a perfect match. To find the roots of the system, a numerical iteration scheme was developed. For this, first of all, two displacement hodographs were built. The values of σ were varied over a small range to find the σ that would minimize the distance between the hodographs (zero distance would mean coincidence). Then, in the periodically repeated simulation mode, the frequency and σ of the hodographs are found. Figure 5 shows how to determine the "root determinant" solution on the complex plane for a particular harmonic under a given tuning condition. Here we found the root of the

hodograph coincidence at a stable $\sigma = -0.014$. This scheme was repeated for each of the frequencies of possible matches over the entire range of debugging conditions.

Figure 6 shows the range of σ and the frequencies at which the hodographs coincide, for a specific setting condition of the SWaAGL-50 machine built in the *s* zone.

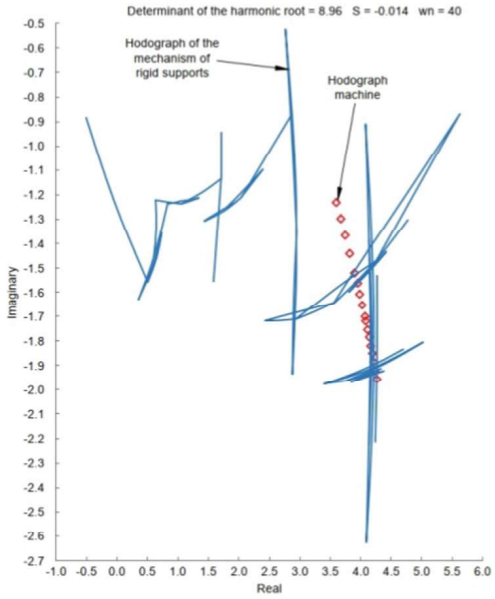

Fig. 5. Iterative "root determinant" scheme of frequency and sigma selection until both hodographs converge in the complex plane.

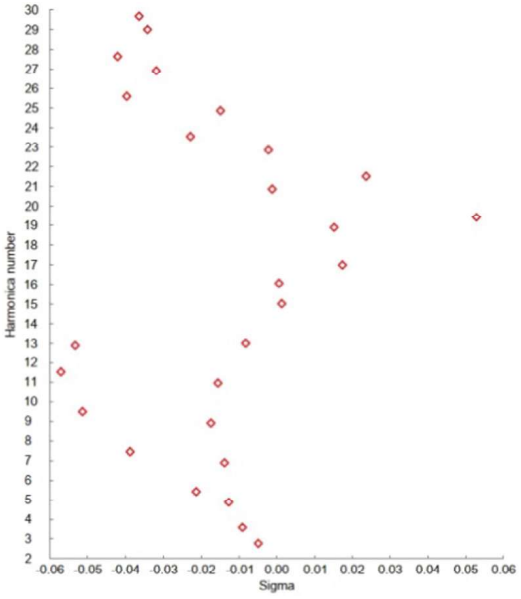

Fig. 6. Characteristic of the roots for one setting condition of the machine.

Any negative σ means that the vibration frequency will not grow exponentially, while any positive σ means unstable growth of the vibration. As can be seen, even and odd frequencies follow stability trends. Even frequency numbers typically remained in the stable range, while odd frequency numbers became unstable from $\frac{\omega}{\omega_n} = 1$ to $\frac{\omega}{\omega_n} = 1.5$, as demonstrated in Fig. 7. As the system approaches instability, from about $\frac{\omega}{\omega_n} = 1$ *to* 1.5, each harmonic has a positive or negative dynamic growth rate. Therefore, in Fig. 7, the spiral has a positive growth rate.

4 Results and Discussion

Summarizing the obtained results, it can be stated that each resonant frequency of the machine can create instability roots for the system, depending on the speed of the part. Both indicators, such as the root of the maximum instability and the total sum of the roots of instability can be used as a parametric estimate of the stability of any particular tuning condition. High frequencies are often damped because the contact length of the grinding wheel with the part is much greater than the effects of these frequencies, resulting in increased stiffness characteristics of the machines. A higher damping of the machine will reduce the size of the instability roots. In this way, better damping will provide better characteristics of the machine regardless of the conditions of its adjustment. The result

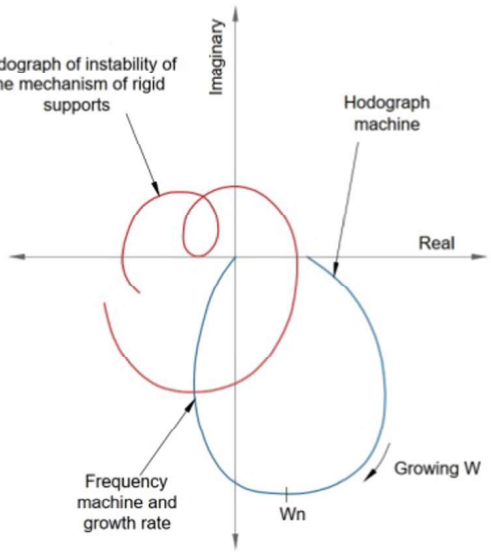

Fig. 7. Explanation of the phenomenon of frequency instability dominance over ω_n: the spiral has a positive growth rate.

of the conducted analysis is the possibility of comparing different debugging conditions from the point of view of the dynamic stability of the machine. The numerical root of the simulations was found for a given machine, each summing up to a general conclusion: that increasing φ_1 and φ_2 within a conventional centerless grinding setup geometry will increase the dynamic stability of the system. Figure 8 shows a contour plot of the root of the maximum instability for each tuning condition within a conventional centerless grinding tuning geometry for a system with a resonant frequency of 100 Hz. Figure 9 shows the root sum for each debugging condition for the SWaAGL-50 machine.

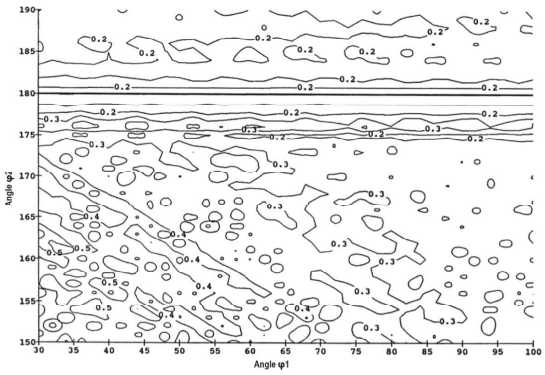

Fig. 8. Contour diagram of the root of maximum instability.

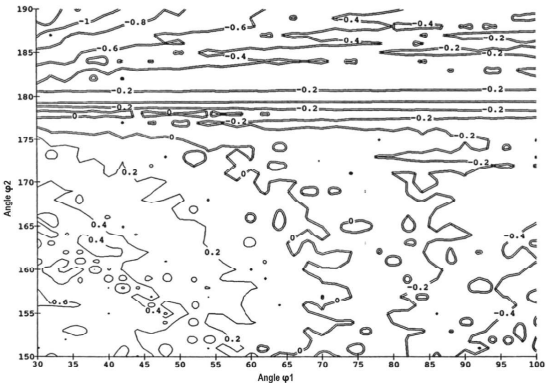

Fig. 9. Contour plot of the total root sum of instability.

The appearance of both diagrams is very similar in that smaller values of φ_1 and φ_2 tend to be more unstable than larger values. One notable exception is for the immediate region near $\varphi_2 = 180°$, which is usually unstable regardless of the value of φ_1. These simulations were performed for machines with different resonant frequencies, with each

result varying slightly in detail. Still, all support the common conclusion presented in Fig. 10, where the darker zones are more unstable than the lighter zones. The general trends proposed by the authors were experimentally confirmed.

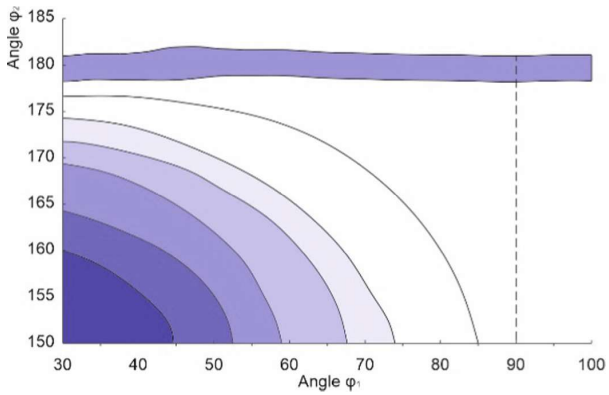

Fig. 10. The main trends of dynamic stability during centerless mortise grinding on rigid supports (the darker the area, the worse dynamic stability it represents).

The conducted research is designed to test theoretical assumptions. A SWaAGL-50 centerless mortise grinding machine on rigid supports was used for this. All grinding variables (speeds, feeds, etc.) were kept constant throughout these studies, except for the two rigid support angles, φ_1 and φ_2.

Changes in the angles φ_1 and φ_2 were made using two mechanisms for adjusting the position of rigid supports. In each position, the rigid supports, which are fixed in place with the help of micrometric screws, ensure positioning stability with an accuracy of 0.25°. For all geometric studies, the part speed was chosen low enough to provide the necessary contact length with the grinding wheel to filter out the machine resonance around 800 Hz. Still, in the vibration growth studies, the part speed was doubled so that this source of vibration was not filtered out.

The confirmed trend is that increasing the angles φ_1 or φ_2 within the normal setup geometry of centerless grinding leads to an increase in the dynamic stability of the MTP system. This trend coincides with theoretical assumptions, which confirm the correlation between the setup geometry and the waviness parameters of the details.

5 Conclusions

Based on the conducted experiments of the MTP system of the SWaAGL-50 machine and the mathematical model and dynamics diagram, it was proven that the vibration of the machine affects the final accuracy of the manufactured part in three ways: 1. The static stiffness of the machine affects the accuracy of the dimensions of the part of the grinding forces excites oscillations in the machine and leads to erroneous dimensional feedback; 2. The geometric effect of setting up rigid supports is strengthened or weakened depending on the low resonant frequencies of the machine; 3. Higher frequency resonances of the machine generate high-frequency irregularities on the part's surface, separately from the geometric regeneration mechanism.

Grinding machines consist of separate components, each of which resonates at one or more separate frequencies. Each resonant frequency of the machine can create the root of instability for the system, depending on the speed of the part. Both indicators, such as the root of the maximum instability and the total sum of the roots of instability, are used as a parametric estimate of the stability of any particular debugging condition. High frequencies are often damped because the contact length of the grinding wheel with the part is much greater than the effects of these frequencies, resulting in increased stiffness characteristics of the machines. Increasing the damping of the machine reduces the magnitude of the roots of instability, arguing that better damping will provide better machine performance regardless of setup conditions. An increase in the angles of rigid supports φ_1 and φ_2 within the normal configuration geometry of centerless grinding increases the dynamic stability of the system. One notable exception is for the immediate region near $\varphi_2 = 180°$, which is usually unstable regardless of the value of φ_1.

References

1. Tuan, N.A.: The effects of process parameters on workpiece roundness in the shoe-type centerless grinding operation for internal raceway of ball bearings. Coatings **13**, 1864 (2023). https://doi.org/10.3390/coatings13111864
2. Wang, X., Li, X., Ma, X., et al.: Advance on surface finishing technology of precision bearing cylindrical rollers. Int. J. Adv. Manuf. Technol. **131**, 2341–2363 (2023). https://doi.org/10.1007/s00170-023-11595-8
3. Badovskyi, O., Balaniuk, A., Oborskyi, G., Orgiyan, A., Edl, M.: An increase in the vibration resistance of finishing and boring machines when cutting ends using the plunge-in method. In: Ivanov, V., Trojanowska, J., Pavlenko, I., Rauch, E., Piteľ, J. (eds.) DSMIE 2024. LNME, pp. 139–151. Springer, Cham (2024). https://doi.org/10.1007/978-3-031-61797-3_12
4. Tuan, N.A.: Multi-objective optimization of process parameters to enhance efficiency in the shoe-type centerless grinding operation for internal raceway of ball bearings. Metals **11**, 893 (2021). https://doi.org/10.3390/met11060893
5. Leonesio, M., Wojcicki, J., Bianchi, G.: Geometrical optimization of centerless grinding process by profiled workrest. Int. J. Adv. Manuf. Technol. **114**, 3069–3075 (2021). https://doi.org/10.1007/s00170-021-07040-3
6. Patil, R.B., Al-Dahidi, S., Newale, S., Arezki Mellal, M.: Reliability analysis of centerless grinding machine using fault tree analysis. In: Kumar, V., Pham, H. (eds.) Predictive Analytics in System Reliability. SSRE, pp. 191–211. Springer, Cham (2023). https://doi.org/10.1007/978-3-031-05347-4_13
7. Chalyj, V., Moroz, S., Ptachenchuk, V., Zablotskyj, V., Prystupa, S.: Investigation of waveforms of roller bearing's working surfaces on centerless grinding operations. In: Ivanov, V., Trojanowska, J., Pavlenko, I., Zajac, J., Peraković, D. (eds.) DSMIE 2020. LNME, pp. 349–360. Springer, Cham (2020). https://doi.org/10.1007/978-3-030-50794-7_34
8. Chalyj, V., Moroz, S., Tkachuk, A., Zablotskyi, V., Trokhymchuk, I., Stelmakh, A.: Formation of bearings parts waviness in centerless mortise grinding on rigid supports. J. Eng. Sci. **10**(1), A15–A21 (2023). https://doi.org/10.21272/jes.2023.10(1).a3
9. Simonovskiy, V., Pavlenko, I., Pitel, J., Stremoukhov, D., Ivanov, V.: Methods and algorithms for calculating nonlinear oscillations of rotor systems. In: Ivanov, V., Pavlenko, I., Liaposhchenko, O., Machado, J., Edl, M. (eds.) DSMIE 2021. LNME, pp. 63–74. Springer, Cham (2021). https://doi.org/10.1007/978-3-030-77823-1_7

10. Pavlenko, I., Verbovyi, A., Neamţu, C., Ivanov, V., Ciszak, O., Trojanowska, J.: Fractional-order mathematical model of single-mass rotor dynamics and stability. Alex. Eng. J. **76**, 91–100 (2023). https://doi.org/10.1016/j.aej.2023.06.024
11. Janmanee, P., Butdee, S.: Spindle Vibration prediction for the CNC machining center using ANFIS system. In: Ivanov, V., Trojanowska, J., Pavlenko, I., Rauch, E., Piteľ, J. (eds.) DSMIE 2024. LNME, pp. 212–222. Springer, Cham (2024). https://doi.org/10.1007/978-3-031-61797-3_18
12. Gavlas, M., et al.: Research on the oscillation in centerless grinding technology when machining bearing steel. Materials **15**, 4968 (2022). https://doi.org/10.3390/ma15144968
13. Lishchenko, N., O'Donnell, G., Larshin, V., Mochuliak, A., Uminsky, S.: Just in time gear grinding wheel dressing. In: Ivanov, V., Trojanowska, J., Pavlenko, I., Rauch, E., Piteľ, J. (eds.) DSMIE 2023. LNME, pp. 297–306. Springer, Cham (2023). https://doi.org/10.1007/978-3-031-32767-4_28
14. Kunitsyn, M., Usov, A., Zaychyk, Y.: The influence of cutting forces on cracks formation during the grinding of products from materials prone to defect formation. In: Ivanov, V., Trojanowska, J., Pavlenko, I., Rauch, E., Piteľ, J. (eds.) DSMIE 2024. LNME, pp. 240–250. Springer, Cham (2024). https://doi.org/10.1007/978-3-031-61797-3_20